Airborne Laser Profiling of Swell in an Open Ice Field

PETER WADHAMS

Scott Polar Research Institute, University of Cambridge, Cambridge, England

Airborne laser profiles of swell entering the drift ice off the east coast of Newfoundland were made using a Geodolite profiler mounted in a DC-4 ice patrol aircraft. Concurrent infrared imagery along the track enabled the floe size distribution to be recorded. A linear decay of wave energy with 'effective penetration' (distance penetrated multiplied by fractional ice cover) was found, the decay rate increasing with wave frequency. A simple theoretical model based on progressive reflection from rows of floes gave good agreement with the observations.

INTRODUCTION

When ocean waves enter an ice field, they are rapidly attenuated, but the mode of amplitude decay depends on the nature of the ice cover. In the central Arctic basin, where the ice cover is virtually a continuous sheet, a wave can become coupled to the ice and can propagate over great distances as a very low amplitude flexural gravity wave until it is finally dissipated by creep [*Wadhams*, 1973*a*]. The surface oscillations due to these waves have been measured by gravity meters mounted on the ice [*Hunkins*, 1962; *LeSchack and Haubrich*, 1964], by seismographs [*Sytinskiy and Tripol'nikov*, 1964] and tiltmeters [*Smirnov and Lin'kov*, 1971]. A different ice morphology is found in the fringes of the Arctic ice cover open to the Atlantic and in coastal drift ice fields, such as those of Labrador and East Greenland, where ice that has been carried down by a cold current predominates over locally generated ice. Here the cover consists of discrete floes of moderate size which behave as independent rigid floating rafts and scatter the incident wave energy. The energy thus scattered or reflected either reemerges from the front of the ice field or else is lost within the ice field by various dissipative processes.

The measurement of wave amplitude decay in this open type of ice field is more difficult than in either the open sea or a continuous cover. *Robin* [1963] employed a ship-borne wave recorder mounted on a surface vessel, but this has the disadvantages that the ice field is disturbed by the vessel's entry and that the recording may not be valid if the vessel is beset or is unduly influenced by the motions of the floe nearest to it. Measurements have also been made using an inverted echo sounder mounted on a submerged submarine [*Wadhams*, 1972], but here the advantage of remote sensing is offset by the difficulty of recording the nature of the ice cover passing overhead. A successful technique should combine remote sensing with the simultaneous recording of floe sizes and concentrations. These requirements can be fulfilled by using an airborne laser profiler to record the sea surface elevation with concurrent imagery of ice conditions along the track from infrared line scanning(IRLS) or overlapping aerial photography. Just such a combination of instruments was to be found in the DC-4 ice patrol aircraft used by the Atmospheric Environment Service of the Department of the Environment, Canada; and in June 1972 the author carried out some observations from one of these aircraft (CF-KAE) during its regular missions off the coasts of Newfoundland and Labrador.

TECHNIQUE OF OBSERVATION

The DC-4 aircraft used at that time had been modified for ice reconnaissance as described by *Archibald* [1972] and were fitted with a Spectra-Physics Geodolite 3A laser profiler and a Bendix LN-2 infrared line scanner. The profiler employs a continuous wave He-Ne laser beam, the intensity of which is sinusoidally modulated by an electrooptical modulator. The phase shift between the modulations on the transmitted and received signals provides a measure of the range to the target. At the highest modulation frequency a phase shift of 2π corresponds to a range change of 3.05 m (10 ft); the vertical accuracy is about 20 mm, and the vertical resolution is much better than this over a limited height differential. The horizontal resolution is determined by the 95% response time of the circuitry to a step function range alteration; this was set to 100 ms during the observations, giving a range of 7.6 m over which features such as the edge of an ice floe would be smoothed out and a wave period of 3.1 s (wavelength 15.2 m) below which 50% or more wave smoothing occurs. Laser profilers have been used extensively to measure the topography of continuous ice covers [*Ketchum*, 1971; *Ketchum and Wittman*, 1972] and have recently supplanted the narrow beam radar altimeter [*Barnett and Wilkerson*, 1967; *Darbyshire*, 1970] as a means of recording wave growth in the open sea [*Schule et al.*, 1971].

The infrared line scanner [*Harwood*, 1969] scans the scene passing below in a stripwise fashion using a mirror revolving on a horizontal axis at 100 Hz. The intensity of radiation in the 3 to 5-m band is recorded as an optical analog on film. Ice is discriminated against water mainly because of its lower emissivity. From a height of 305 m the scanner produces imagery of a strip some 700 m wide, centered on the flight track.

For ease of interpretation of the results the aircraft must be aligned with the propagation vector of a distinct unidirectional swell. This imposes stringent limitations on the physical conditions which will permit a profile to be made. The direction of the swell must be easily identifiable from the air, so that it must not be cluttered by cross swells or by a strong local sea. The aircraft follows the swell into the ice on a straight course; therefore the swell should be incident on the ice edge at a low angle of incidence, to avoid errors due to wave refraction. The ice edge itself should be straight and well-defined in the immediate vicinity of the aircraft's point of entry. This requires an on-ice wind, which gathers the small floes in the outer part of the pack into a distinct edge; winds from other directions al-

Present address: Frozen Sea Research Group, Department of the Environment, Victoria, British Columbia, Canada.

Fig. 1. Canadian Atlantic coast. Schematic diagram of surface current directions and extent of drift ice in early June 1972.

low sinuous belts of ice to drift away from the main edge. The pack inside the ice edge should be fairly open, so that a line track across it encounters at least 50% open water; this enables the sea surface to be reconstructed from the laser profile by interpolation across the short sections of ice. Finally, of course, the atmosphere below the aircraft must be free of undercast haze or cloud.

Figure 1 shows the approximate extent of drift ice on the Canadian Atlantic coast in early June 1972. At this time of year the ice is at its maximum advance, under the influence of the Laborador Current, preceding a swift retreat. During its ice patrol missions the aircraft followed the outer ice edge southward from 55°N down to its southernmost lobe. If an approximation to the desired conditions occurred, the aircraft would turn out to sea, descend to 305 m, and align itself antiparallel to the swell vector. Some 20 km outside the ice edge the aircraft would turn through 180° and make any final correction necessary for alignment with the swell vector. The laser, which had already been turned on to warm up, was set to record. After crossing the ice edge the aircraft held its course for 80 km or until all apparent trace of wave action had vanished from the craft record. Course correction within the ice was not possible due to absence of visible swell. Precision navigational fixes were obtained every 2 min from the Bendix Döppler navigational system, which was coupled to a Minac 5 latitude/longitude computer [*Archibald*, 1972]. A height of 305 m (1000 ft) was found to be the minimum for steady porpoising of the aircraft without 'bumping'; rolling of the aircraft was undetectable. The sea ice distribution was recorded throughout the run using the IRLS.

By far the best conditions occurred on June 6 (flight KAE866). Figure 2, taken from an ice chart prepared aboard the aircraft, shows the ice conditions and position of the ice edge. A clearly delineated swell was observed heading at 220° directly into the ice field, and a laser run of total length 100 km was obtained before a cloud bank was entered. The laser phase lock failed at the ice edge, and the first 4 km of track within the ice were missed, but otherwise the record was continuous.

Isobaric surface analyses for 1200 and 1800 UT are shown in Figure 3; a ridge of high pressure was moving to the east, and on the basis of the isobars we surmise that a wind of about 2-5 m s^{-1} would have arisen by 1830 UT, the time of the profile. The flight log records a mean wind at 305 m of 9 m s^{-1} from 193°, based on aircraft drift. This leaves a wide range of possibility for the wind at anemometer height; we suggest a value of about 5 m s^{-1} from ahead (220°), but a drawback of the laser technique is that this important quantity cannot be accurately determined unless a ship is stationed in the area at the same time.

NATURE OF THE LASER WAVE SPECTRUM

Spectral analysis of a laser profile obtained from a moving aircraft yields in the first instance a wave number spectrum,

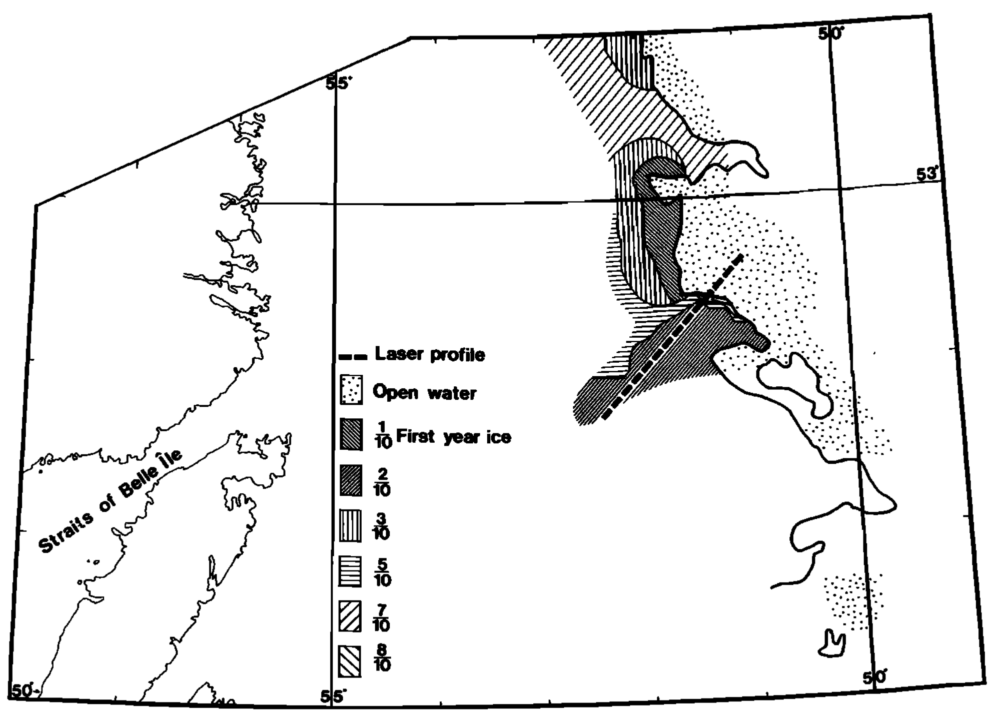

Fig. 2. Ice conditions and position of ice edge in neighborhood of laser run, June 6, 1972.

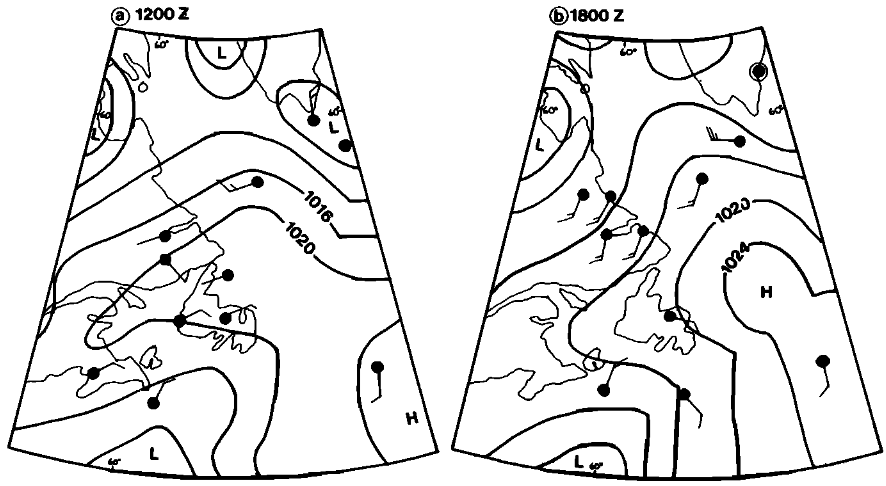

Fig. 3. Isobaric surface analyses for 1200 and 1800 UT, June 6, 1972.

but since the aircraft velocity is finite, this is a 'spectrum of encounter' [*Cartwright*, 1963] rather than a true spectrum. We now discuss the conversion of such a spectrum into a true wave number spectrum and then into a frequency spectrum. The problem was first tackled by *St. Denis and Pierson* [1953] for spectra observed from moving ships and later by *Barnett and Wilkerson* [1967] in a different way for their aircraft observations.

A spatial profile $y(s)$, extending from $s = 0$ to S, can be analyzed to yield a finite Fourier transform

$$x(\kappa_m, S) = h \sum_{n=0}^{n-1} y_n \exp\left(\frac{-i2\pi m}{N}\right) \qquad (1)$$

$$m = 0, 1 \cdots N-1$$

where the record consists of N points y_n spaced h apart. If the fast Fourier transform (FFT) technique is used [*Cooley and Tukey*, 1965], the wave numbers κ_m appear as multiples of a fundamental wave number $1/S$, i.e.,

$$\kappa_m = m/S = m/Nh \qquad m = 0, 1, \cdots N-1 \qquad (2)$$

The power spectral density $G_y(\kappa)$ is estimated by

$$\hat{G}_y(\kappa) = \frac{2}{S} \, |X(\kappa, S)|^2 \qquad (3)$$

We now assume that the wave field is homogeneous, i.e., that stationary wave recorders placed anywhere in the interval $(0, S)$ would record time series having identical statistical properties. In a laser profile the wave energy continually decreases as we move into the ice field, so in our analysis we split the record into continuous sections to be analyzed separately, and we assume homogeneity and stationarity for each section. If $G_x(f)$ is the spectral density of a time series made by one of these imaginary stationary recorders, then the mean square elevation Φ^2 of the sea surface is given by

$$\Phi^2 = \int_0^\infty G_x(f)\, df = \int_0^\infty G_y(\kappa)\, d\kappa \qquad (4)$$

Equation (4) does not enable us to transform from the $(G_y(\kappa), \kappa)$ plane to the $(G_x(f), f)$ plane unless we have some knowledge of the directional properties of the wave energy. This can be easily seen by reference to Figure 4*b*, where a wave train is traveling at an angle Ψ to the line $0S$ along which a spatial profile has been taken. The wave energy appears in the spectrum at a wave number $\kappa = \cos \Psi/\lambda$, whereas a time series recorded at some point along the track will show waves of the same amplitude but with a frequency $f =$ (period of a wave of length $\lambda)^{-1}$. The transformation is therefore a function of Ψ. By flying in the major direction of the swell vector we can assume that the wave energy all travels in the positive s direction, making the transformation simpler. We also assume that the swell has no directional spread; *Barnett and Wilkerson* [1967] found that even for a wind-generated sea a unidirectional assumption gave a corrected spectrum that was very similar to spectra obtained from assumptions of directional spread.

Let κ_a, $G_a(\kappa_a)$ be the apparent wave number and spectral

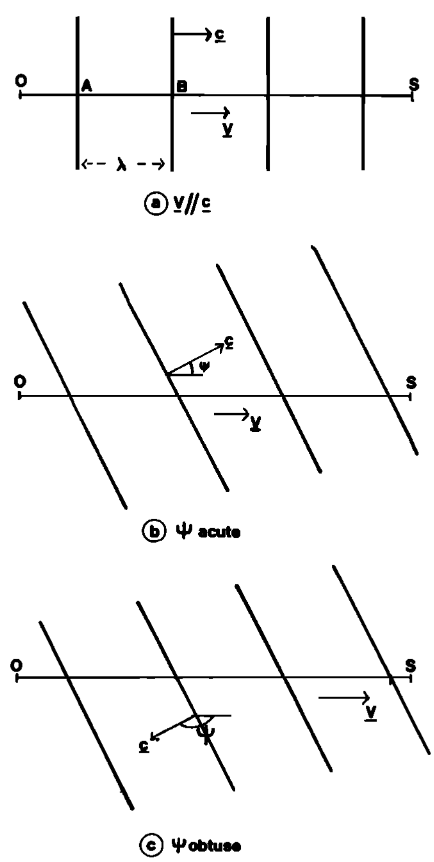

Fig. 4. The geometry of a laser profiling run from 0 to S. V is the aircraft velocity, c the phase velocity of a long-crested swell.

density for a component of the laser profile, and let κ, $G(\kappa)$ be the corrected values. In Figure 4, regarding the component as a sinusoidal long-crested wave,

$$\kappa_a = \kappa\left[\cos\Psi - \frac{1}{V}\left(\frac{g}{2\pi\kappa}\right)^{1/2}\right] \qquad (5)$$

$$0 \le \psi < \cos^{-1}(c/V)$$

and

$$\kappa_a = \kappa\left[\frac{1}{V}\left(\frac{g}{2\pi\kappa}\right)^{1/2} - \cos\Psi\right] \qquad (6)$$

$$\cos^{-1}(c/V) < \Psi \le \pi$$

where **V** is the aircraft velocity and **c** the phase velocity of the component. The case of $\cos\Psi = (c/V)$ corresponds to a wave where the speed of the crests along the projected line $\hat{\mathbf{V}}$ is equal to V, so that the laser records a zero apparent wave number.

The inverse transformation is then

$$\kappa = \frac{\kappa_a}{\cos\Psi} + \frac{g}{4\pi V^2\cos^2\Psi} \cdot\left[1 \pm \left(1 + \frac{8\pi V^2}{g}\kappa_a\cos\Psi\right)^{1/2}\right] \qquad (7)$$

as a solution to (5) and

$$\kappa = \frac{-\kappa_a}{\cos\Psi} + \frac{g}{4\pi V^2\cos^2\Psi} \cdot\left[1 \pm \left(1 - \frac{8\pi V^2}{g}\kappa_a\cos\Psi\right)^{1/2}\right] \qquad (8)$$

as a solution to (6). Equations (7) and (8) are identical if we replace Ψ by $\Psi' = 180° - \Psi$ when $\Psi > \cos^{-1}(c/V)$. Regarding the sign of the discriminant, only the positive solution is feasible in the region $0 \le \Psi < \cos^{-1}(c/V)$ and the negative solution in the region $\cos^{-1}(c/V) < \Psi \le \pi$. There is a singular solution at $\Psi = \pi/2$ of

$$\kappa = 2\pi V^2\kappa_a^2/g \qquad (9)$$

The transformation to a corrected spectrum is given by

$$G = G_a\,(\partial\kappa_a/\partial\kappa)_\Psi \qquad (10)$$

which can be calculated from (7) or (8). In the specific case $\psi = 0$ which is relevant to our results,

$$G = \frac{G_a}{[1 + (1 + 8\pi V^2\kappa_a/g)^{-1/2}]} \qquad (11)$$

Finally, to convert to a frequency spectrum, we note that for corresponding narrow bands, $\partial\kappa$, ∂f in the two spectra,

$$G(f)\,\partial f = G(\kappa)\,\partial\kappa \qquad (12)$$

Using the relations for deep water and proceeding to the limit, we obtain

$$G(f) = G(\kappa)(8\pi\kappa/g)^{1/2} \qquad (13)$$

where

$$f = (g\kappa/2\pi)^{1/2} \qquad (14)$$

If the aircraft falls off from the direction of the swell so that Ψ increases, the apparent wave number and frequency of every component will decrease, since by (5),

$$(\partial\kappa_a/\partial\Psi)_\kappa = -\kappa\sin\Psi \qquad (15)$$

This suggests that if the wave energy has directional spread about its mean vector this will cause errors in the spectral analysis. In Figure 5*a*, κ_a and κ are apparent and corrected spectra for a unidirectional sea moving parallel to the aircraft. If the sea has a finite angular spread which is not frequency dependent, then curves such as κ_a' represent contributions from energy traveling at an acute angle Ψ. κ' shows where this appears in the 'corrected' spectrum (corrected, that is, on the basis of $\Psi = 0$). The relative contribution from κ' is significant only to the left of the energy peak of κ. This shows that if a corrected spectrum is calculated on a unidirectional assumption while the sea in reality has angular spread, the result is substantially correct for all wave numbers below that of the main spectral peak. This is provided the aircraft has been accurately aligned with the major axis of the directional spectrum.

Figure 5*b* shows what happens when Ψ is obtuse; when $\Psi = 180°$, for instance, we are dealing with energy backscattered (reflected) from the floes. If the backscattered spectrum of encounter has a peak at κ_C' (apparent), transforming to κ_D' (corrected on the basis of $\Psi = 0$), which corresponds to waves of the same frequency as κ_A and κ_B in the forward spectra, then manipulation of (5) and (6) yields

$$(\kappa_D')^{1/2} - (\kappa_B)^{1/2} = (g/2\pi V^2)^{1/2} \qquad (16)$$

With $V = 76.2$ m s^{-1} we find that a κ_B corresponding to $T = 10$ s gives a κ_D' at $T = 8.3$ s. This is not a sufficient shift to completely separate the backscattered from the forward spectra. Therefore a measured spectral component is liable to be contaminated with reflected energy from a longer wave period. However, in the following analysis we assume the relative contribution of reflected energy to be negligible.

ANALYSIS OF RESULTS

Ice conditions. The IRLS record from the run of June 6 was marked off in 1-km sections, and a 100-m-wide band of each section was examined under a traveling microscope whose graticule was calibrated directly in meters from the known scaling factors involved. The band was centered on the midline of the record, since this is the actual laser track and the

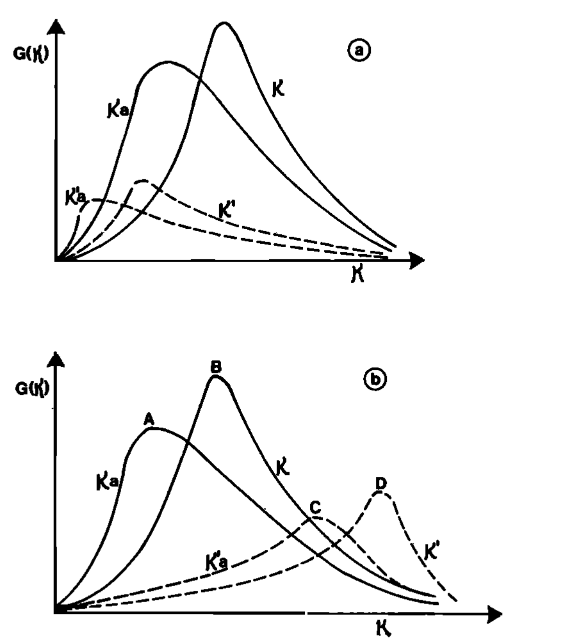

Fig. 5. Apparent and true wave number spectra.

lateral distortion due to the geometry of the scanning process is least in the center. Floes were counted and ascribed to size classes depending on their extreme cross-track width; the classes were in steps of 5 m up to 20 m and 10 m thereafter. Cakes less than 1 m in diameter were difficult to resolve against defects of the print and were ignored; otherwise all floes were counted that had their centers of gravity within the 1 km $\times$ 100 m rectangle. The total percentage ice cover was calculated using a mean diameter for each class. The results are shown in Figure 6, broken down into total cover and cover due to floes more than 20 m across: the most noteworthy feature is the high concentration of ice in the outermost 15 km of pack as compared to its openness further inside.

Conditions varied most rapidly in the outermost 1 km, and this was examined more closely in 100-m-long sections, using a 200-m width to improve the statistics. Figure 7 shows that the first 200 m are composed entirely of small cakes less than 10 m across, after which the proportion of larger floes gradually builds up.

The mean thickness of the ice can only be guessed at. The ice observers' chart (Figure 2) describes the whole area as being composed of first-year ice; and at this time of year such ice in the area has been estimated to have a mean thickness of 1.3 m [*Dinsmore,* 1972] and 1.3–1.5 m [*Markham,* 1969]. However, the larger floes sometimes display considerable structure in the infrared, with 'warm' dark spots, probably consisting of meltwater pools, and 'cold' white areas, which may correspond to hummocks. This suggests that some of the larger floes, at least, may be multiyear ice (probably from Foxe Channel), in which case the thickness may be up to 2 m.

Laser profiles. The laser profiles were recorded on UV sensitive paper as an analog record with a full-scale deflection corresponding to 3.05 m; if the range varied by more than this amount, the trace jumped automatically back across to zero.

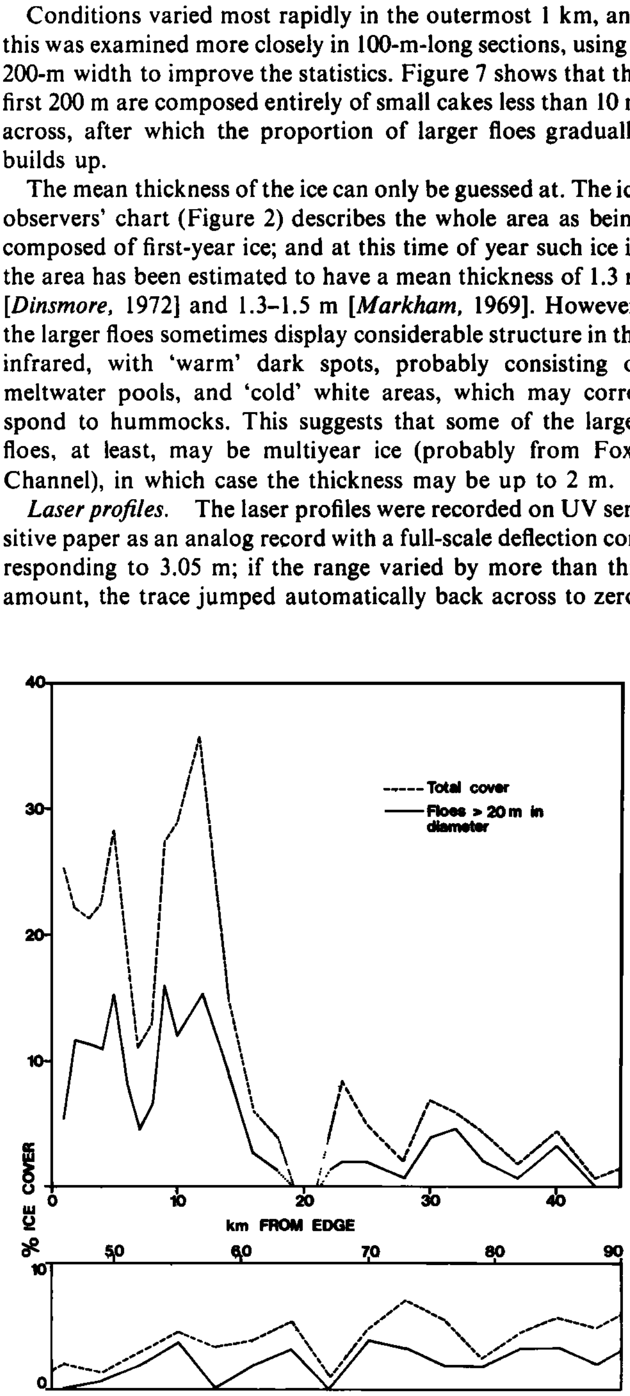

Fig. 6. Percentage of sea surface covered by ice along laser track, as determined by infrared scanning, June 6, 1972. Record is in two sections.

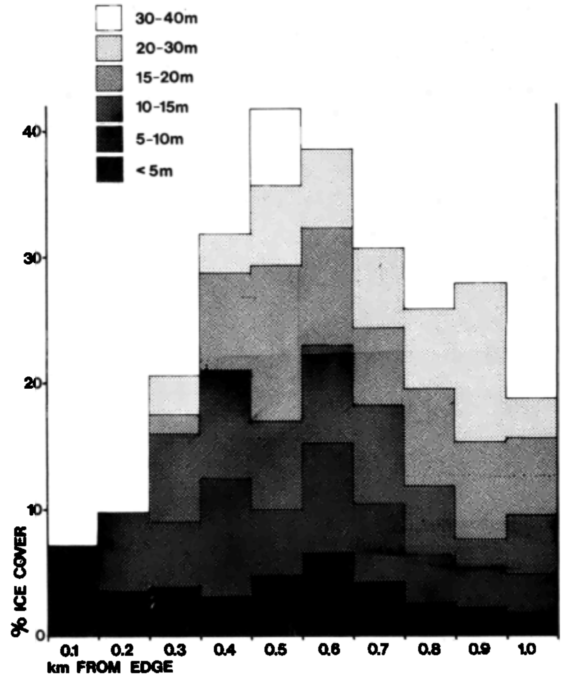

Fig. 7. Distribution of floe diameters in the outermost kilometer of ice field.

The complete record was digitized using a curve follower, and the phase jumps were removed. The openness of the ice field and small size of floes meant that the sea surface could be reconstructed across the 'blips' on the record which correspond to floes; this avoids introducing noise into the spectrum through digitization of the ice surface. Aircraft porpoising was removed by running an FFT on the whole record and constructing a low-pass profile, based on the amplitudes and phases of all Fourier components with periods greater than 80 s, which was then subtracted from the raw record. The porpoising appeared quite regular, so that the more elaborate filtering technique of *Hibler* [1972] was unnecessary. It is possible that shorter-period porpoising did remain in the record, although imperceptible to the naked eye. If so, it is reasonable to expect it to be a homogeneous process (in the absence of obvious patches of turbulence), giving equal energy contributions at all penetrations.

The record was now divided into 10 sections, each of length 10.03 km; sections 1 and 2 were in open water, while 3–10 were within the ice field, section 3 beginning 4.3 km inside the ice edge on account of the loss of phase lock. Each section was linearly interpolated so as to consist of 512 points spaced 19.6 m apart, and the mean and linear trend were removed. The end tenths of each section were tapered, so as to reduce side lobe leakage in the subsequent spectral analysis, using the data window of *Bingham et al.* [1967]:

$$\begin{array}{ll} \frac{1}{2}\left[1 - \cos\frac{\pi s}{0.1S}\right] & 0 \le s \le 0.1S \\ 1 & 0.1S < s < 0.9S \\ \frac{1}{2}\left[1 - \cos\frac{\pi(S-s)}{0.1S}\right] & 0.9S \le s \le S \end{array} \qquad (17)$$

An FFT was run on each section, and the spectral energy densities were estimated from (1) and (3). The spectral estimates were multiplied by 1/0.875 to compensate for the effect of the tapering.

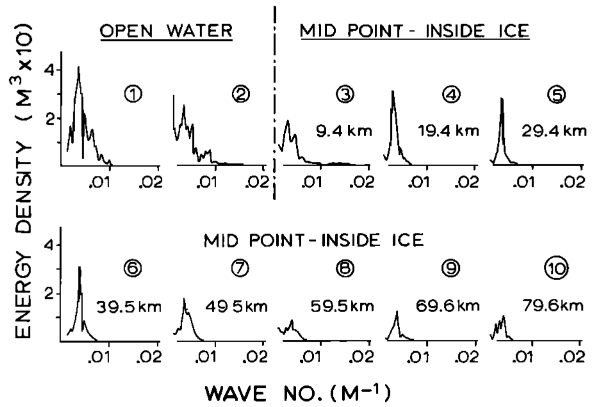

Fig. 8. Spectra of encounter. Successive 10.03-km sections of track are numbered 1 to 10, distances shown being position of midpoint related to ice edge.

Figure 8 shows the results for the spectrum of encounter, smoothed by averaging over four of the intervals defined in (2). Averaging over n intervals gives a normalized standard error ϵ_r in each spectral estimate of approximately

$$\epsilon_r = 1/n^{1/2} \tag{18}$$

so in this case the error is $\pm 50\%$. In Figure 9 the spectra have been corrected for aircraft motion using (7) and (11) and transformed to a frequency spectrum using (13) and (14). The spectra are very sharply peaked, a consequence of the regularity of the swell.

The 'true' frequency of the major peak was assumed to remain constant from spectrum to spectrum, and the small fluctuations found in the analyzed results were ascribed to navigational drift (equation (15)) or variations in ground speed; variations of up to 5% about the mean of 76.2 m s^{-1} were recorded in the flight log, but as these were estimated between fixes only 2 min ($\simeq$9 km) apart, the scatter may be a statistical artifact. The energy at the major peak was estimated by integrating over a 14-interval spectral band centered on the peak of each spectrum. This produces a standard error of roughly $\epsilon_r = 1/14^{1/2} = 27\%$. The rest of the spectral range was divided into standard 14-interval bands, the central frequencies of which are defined in Table 1. The mean energy in each band was calculated by using the corrected wave number spectrum (given by (11)) and then converting the mean density into a density with respect to frequency space using (13). Since the wave numbers (but not the frequencies) are uniformly spaced, this avoids biasing in the mean. Figure 10 shows the resulting energies plotted against the position of the midpoint of each record section relative to the ice edge.

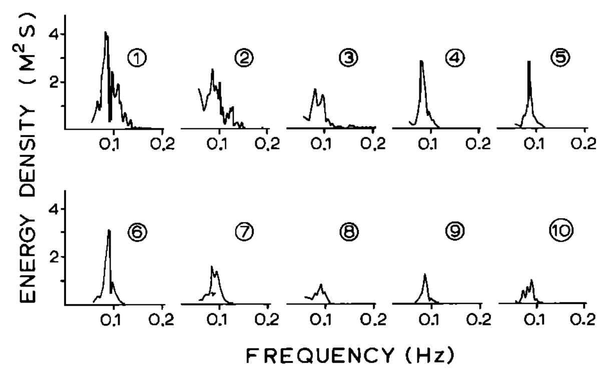

Fig. 9. Corrected frequency spectra.

TABLE 1. Amplitude Attenuation Coefficients

Wave Band	Central Period, s	α_{x_e}, 10^{-4} m^{-1}
Peak	11.6 ± 0.1	1.2 ± 0.2
3	10.53	1.3 ± 0.2
4	9.35	2.7 ± 0.1
5	8.50	3.5 ± 0.1
6	7.85	4.4 ± 0.2
7	7.34	5.2 ± 0.2

The results do not suggest a clear trend except for a more rapid attenuation at high frequencies. However, we have not yet taken account of the variability of the ice cover. We can replace distance of penetration x by an 'effective penetration' x_e, obtained by integrating under the total ice cover curve of Figure 6. Thus

$$x_e = \int_0^x P_z \, dz \tag{19}$$

where p_z is the fraction of sea surface covered by ice at penetration z. Then x_e represents the distance that the wave would have to penetrate were the ice between 0 and x to be pushed up together into a 100% cover. If we now plot the mean energy against x_e rather than x (Figure 11), we find that the energy decay has an exponential form, except for a systematic positive

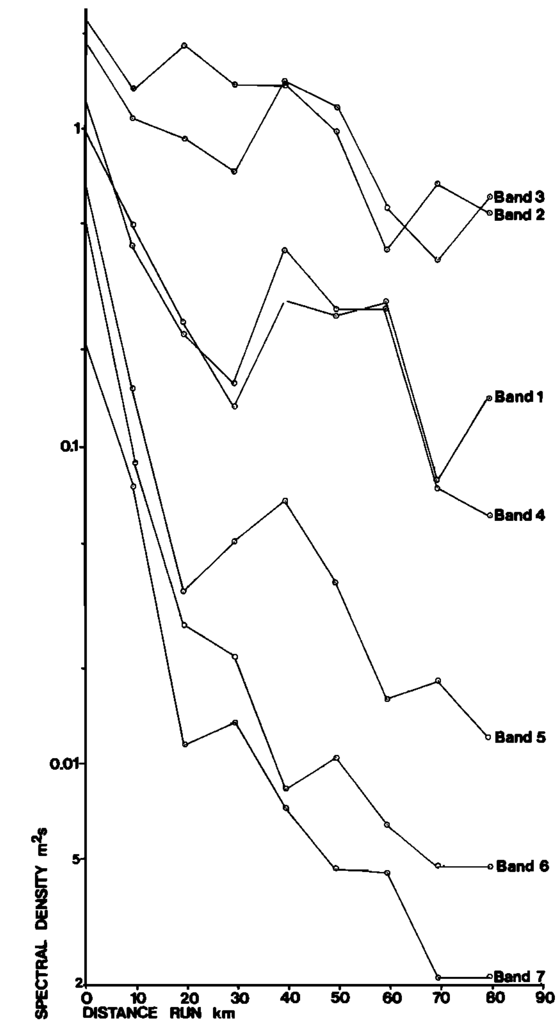

Fig. 10. Energy density plotted against midpoint of record segment.

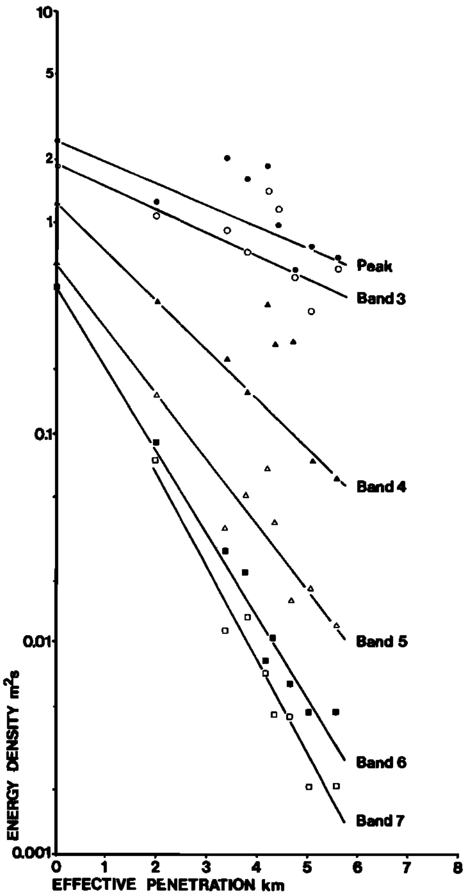

Fig. 11. Energy density against 'effective' penetration.

deviation at about 40-km penetration. An amplitude attenuation coefficient α_{x_e} can be defined for an exponential decay by

$$G_{x_e}(f) = G_0(f) \exp(-2\alpha_{x_e} x_e) \qquad (20)$$

where $G_{x_e}(f)$ and $G_0(f)$ are energy densities at x_e and at the ice edge, respectively. Table 1 gives the values of α_{x_e} for the different wave bands calculated from two-parameter regression lines fitted to Figure 11, neglecting the points with large positive deviations which we attempt to explain in the next section. Bands 1 and 2 have also been neglected, since their periods are longer than the major peak, for the reason discussed in the previous section.

Figure 12 is a log-log plot of α_{x_e} against wave period T. Apart from the two longest periods, the results appear to fit an empirical power law

$$\alpha_{x_e} = Kf^n \qquad (21)$$

over the range of the observations, fitted by regression, where n is (2.70 ± 0.05) and K is $(2.2 \pm 0.2) \times 10^{-2}$. If any short-period porpoising remained in the record, it would tend to reduce α, since energies would be increased by absolutely (but not relatively) equal amounts at each penetration.

DISCUSSION

A laser profile occupies a considerable linear distance, and in an open ice field much of the water surface is exposed to the wind, so we must first consider whether the wave energy could be modified by environmental factors unconnected with ice. The possible factors involved are (1) losses due to molecular viscosity in the body of the water, (2) the addition to the spectrum of a local wind-generated sea, (3) loss of energy from the swell due to interaction with the local sea, and (4) loss of energy from the swell due to direct coupling with an adverse wind.

Effect 1 gives an attenuation coefficient [*Lamb*, 1932] of

$$\alpha_x = 8\pi\nu k^2 f/g \qquad (22)$$

where $k = 2\pi/\lambda$ and ν is kinematic viscosity. This is of order 10^{-9} m^{-1} and so is negligible.

The wind was slight and blowing from the land, so that effect 2 is not likely to be significant. It may account for the positive deviations of energy observed in Figure 10 at about 40-km penetration. The head sea would be greater at moderate penetration (where the fetch is longer) than at deep penetration, but it would tend to disappear at low penetrations as it encounters denser ice cover on the way out of the ice field.

Hasselmann [1971] showed that the interaction in effect 3 is mainly with very short waves of wavelength less than 0.35 m; the attenuation rate in a moderate sea is less than 10^{-5} m^{-1}, and in a light sea it would be much less. There have been no adequate measurements of effect 4, which is poorly understood. On the basis of existing theories of wave growth, *Phillips* [1966, chap. 4] predicted values of about 0.5×10^{-4} m^{-1} for α_x in an adverse wind of 5 m s^{-1}. These would be substantial in comparison with our observed rates, but there is no way of telling whether the wind is that strong at the surface. Further, no significant decay was observed over the open water sections of the profile, so we tentatively conclude that both 3 and 4 are negligible in relation to the effect of the ice.

These decay rates, together with the precise information on floe size distributions, furnish material to test models of the decay process. The major mechanism of attenuation is un-

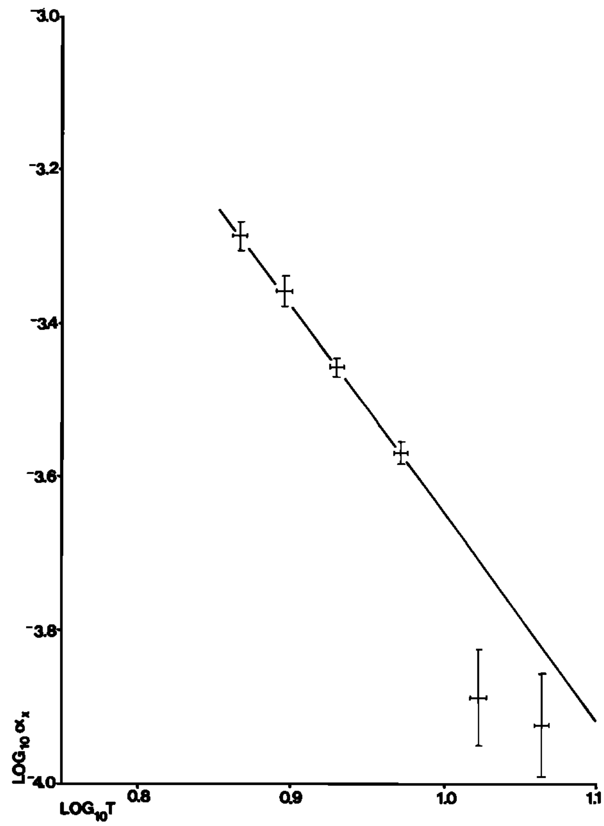

Fig. 12. Log-log plot of amplitude attenuation coefficient against wave period.

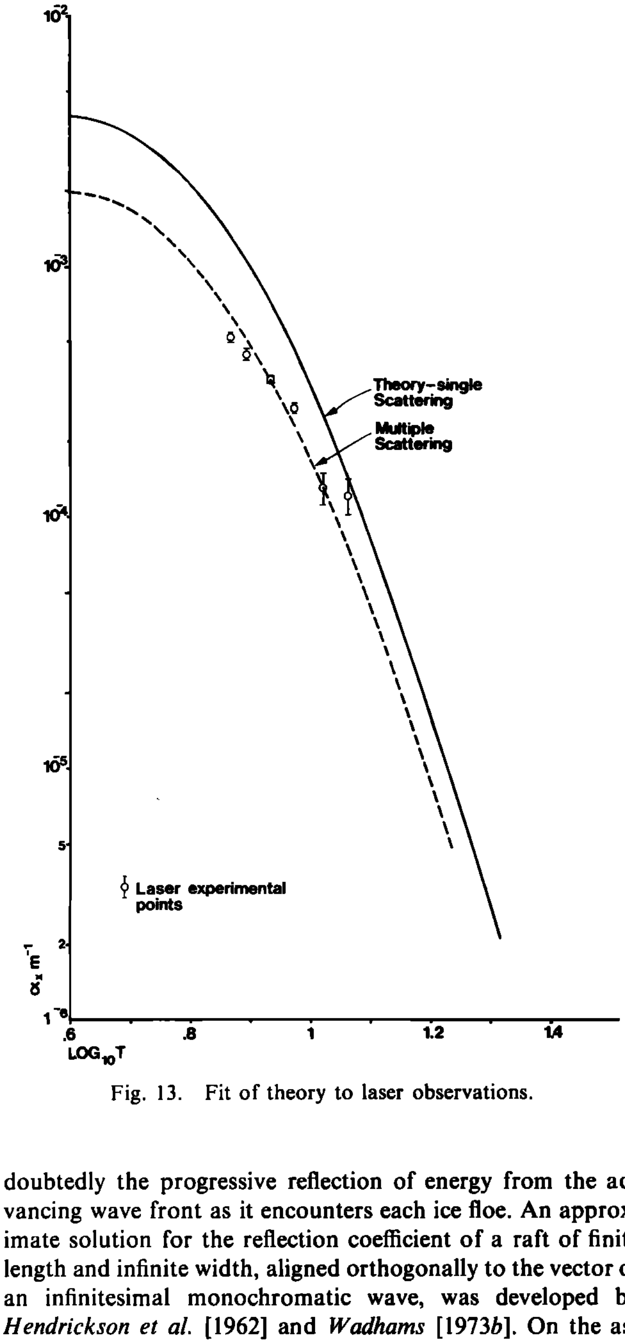

Fig. 13. Fit of theory to laser observations.

doubtedly the progressive reflection of energy from the advancing wave front as it encounters each ice floe. An approximate solution for the reflection coefficient of a raft of finite length and infinite width, aligned orthogonally to the vector of an infinitesimal monochromatic wave, was developed by *Hendrickson et al.* [1962] and *Wadhams* [1973*b*]. On the assumption of irrotational flow in an inviscid incompressible fluid of infinite depth, a solution for the velocity potential under the floe was found as the sum

$$\phi = \sum_n [A_n e^{ik_n x} + B_n e^{-ik_n x}] e^{-k_n y} e^{-i\omega t} \tag{23}$$

where x is measured along the wave vector and y downward from the surface. This satisfies the boundary conditions if

$$Lk_n^5 + (\rho_w g - \rho_i h\omega^2)k_n - \rho_w \omega^2 = 0 \tag{24}$$

where h is the floe thickness (although zero depth of submergence is assumed), ρ_w, ρ_i are water and ice densities, and L is the flexural rigidity given by

$$L = Eh^3/12(1 - \gamma^2) \tag{25}$$

with E as Young's modulus and γ as Poisson's ratio for the ice. There are three physically feasible solutions for k_n:

$$\begin{aligned} k_0 &\neq k \qquad (k = 2\pi/\lambda = \omega^2/g) \\ k_1 &= a + bi \\ k_2 &= a - bi \end{aligned} \tag{26}$$

where k_0, a, and b are real and positive. Beneath the front and rear floe edges the transition condition to a free water surface requires that ϕ and $\partial\phi/\partial x$ be continuous for all y. This is not possible since ϕ in (23) cannot be matched at all depths to a corresponding ϕ_w for open water given, for the front of the floe, by

$$\phi_w = [A_w e^{ikx} + B_w e^{-ikx}] e^{-iky} e^{-i\omega t} \tag{27}$$

where $|B_w|^2/|A_w|^2 = r$, the energy reflection coefficient from the floe edge. Additional potentials of different form must exist, but Hendrickson et al. found an approximate solution by matching (23) and (27) only at $y = 0$ and solving numerically to yield r. This approximation should be accepted with caution.

A real ice field contains floes of differing shapes and sizes. Each floe scatters energy in all directions in the x-z plane, but since its induced motion under a long-crested swell is all in the x-y plane, most of the scattered energy will be in the x direction. Hendrickson's model can be applied by picturing the infinitely wide floe as equivalent to a row of roughly square floes, each of diameter d, situated with their centers at the same value of x, so that they all respond in phase to the incident wave. Energy scattered by individual floes in the positive and negative x directions is then reinforced, whereas energy scattered to the side is not. On a single scattering assumption, where the reflected fraction r is considered to be dissipated by some means before reaching another row of floes, the attenuation coefficient is given by

$$\alpha_x = \frac{1}{2} \sum_i \frac{p_i r_i}{d_i} + 0(r_i)^2 \tag{28}$$

where r_i is the reflection coefficient for floes of size class d_i which occupy a fraction p_i of the sea surface area. A somewhat more realistic assumption allows each parcel of energy to suffer up to two reflections, the scattering being incoherent so that the energies of the resulting forward wave can be added arithmetically. In this case, for a single size class,

$$\alpha_x = \frac{p}{2d}\left[r - \frac{r}{2 + (n-1)r} + 0(r^2)\right] \tag{29}$$

when n rows of floes have been crossed. If $(n - 1)r \ll 2$, which is true for the length scale of this experiment, then

$$\alpha_x \doteq pr/4d \tag{30}$$

or half the value given by (28).

Using the floe size distributions given by the IRLS and a value of 1.5 for ice thickness, α_x was computed from (28) and (30) and compared with experiment (Figure 13). The fit in the multiple scattering (two reflection) case is good enough to suggest that this approach provides a reasonable quantitative description of the rate of attenuation of waves in an open ice field.

Acknowledgments. This experiment was made possible by the initiative and cooperation of the Atmospheric Environment Service, Department of the Environment, Downsview, Ontario, and I am especially grateful to H. Hengeveld, W. F. Ganong, T. Kilpatrick, R. Van Humbeck, and the ice observer team in the field. During this period I was supported by a research studentship from the Natural Environment Research Council of Great Britain.

REFERENCES

Archibald, D. C., An aerial ice reconnaissance platform with remote sensors suitable for the Canadian ice reconnaissance program, Proceedings of the International Sea Ice Conference, pp. 229–236, Nat. Res. Counc. of Iceland, Reykjavik, 1972.

Barnett, T. P., and J. C. Wilkerson, On the generation of ocean wind waves as inferred from airborne radar measurements of fetch-limited spectra, *J. Mar. Res., 25*(3), 292–328, 1967.

Bingham, C., M. D. Godfrey, and J. W. Tukey, Modern techniques of power spectrum estimation, *Trans. IEEE Audio Electroacoustics, AU-15*(2), 56–66, 1967.

Cartwright, D. E., The use of directional spectra in studying the output of a wave recorder on a moving ship, in *Ocean Wave Spectra*, pp. 203–218, Prentice-Hall, Englewood Cliffs, N. J., 1963.

Cooley, J. W., and J. W. Tukey, An algorithm for the machine calculation of complex Fourier series, *Math. Comput., 19*, 1965.

Darbyshire, J., Wave measurements with a radar altimeter over the Irish Sea, *Deep Sea Res., 17*, 893–901, 1970.

Dinsmore, R. P., Ice and its drift into the North Atlantic Ocean, Symposium on Environmental Conditions in the NW Atlantic 1960–1969, *Spec. Publ. 8*, pp. 82–128, Int. Comm. for NW Atlantic Fish., Dartmouth, Nova Scotia, 1972.

Harwood, T. A., Remote sensing of ice in navigable waters, in *Ice Seminar*, pp. 95–104, Can. Inst. of Mining and Met., Calgary, Alberta, 1969.

Hasselmann, K., On the mass and momentum transfer between short gravity waves and larger-scale motions, *J. Fluid Mech., 50*, 189–205, 1971.

Hendrickson, J. A., L. M. Webb, and R. J. Quigley, Study of natural forces acting on floating ice fields, *Rep. NBy-32215*, 71 pp., Nat. Eng. Sci. Co., Pasadena, Calif., 1962.

Hibler, W. D., III, Removal of aircraft altitude variation from laser profiles of the Arctic ice pack, *J. Geophys. Res., 77*(36), 7190–7195, 1972.

Hunkins, K., Waves on the Arctic Ocean, *J. Geophys. Res., 67*(6), 2477–2489, 1962.

Ketchum, R. D., Jr., Airborne laser profiling of the Arctic pack ice, *Remote Sensing Environ., 2*, 41–52, 1971.

Ketchum, R. D., Jr., and W. I. Wittman, Recent remote sensing studies of the East Greenland pack ice, Proceedings of the International Sea Ice Conference, pp. 213–226, Nat. Res. Counc. of Iceland, Reykjavik, 1972.

Lamb, H., *Hydrodynamics*, 6th ed., 738 pp., Cambridge University Press, London, 1932.

Leschack, L. A., and R. A. Haubrich, Observations of waves on an ice-covered ocean, *J. Geophys. Res., 69*(18), 3815–3821, 1964.

Markham, W. E., Growth, break-up and movement of ice in Canadian coastal waters, in *Ice Seminar*, pp. 31–35, Can Inst. of Mining and Met., Calgary, Alberta, 1969.

Phillips, O. M., *The Dynamics of the Upper Ocean*, 261 pp., Cambridge University Press, London, 1966.

Robin, G. de Q., Wave propagation through fields of pack ice, *Phil. Trans. Roy. Soc. London, Ser. A., 255*(1057), 313–339, 1963.

St. Denis, M., and W. J. Pierson, On the motion of ships in confused seas, *Soc. Nav. Architects Mar. Eng. Trans., 61*, 332–357, 1953.

Schule, J. J., Jr., L. S. Simpson, and P. S. Deleonibus, A study of fetch-limited wave spectra with an airborne laser, *J. Geophys. Res., 76*(18), 4160–4171, 1971.

Smirnov, V. N., and E. M. Lin'kov, Tiltmeter observations of sea-ice oscillations, in *Studies in Ice Physics and Ice Engineering*, edited by G. N. Yakovlev, Gidrometeorologicheskoe Izdatel'stvo, Leningrad. (English translation, pp. 184–190, Israel Program for Scientific Translations, Jerusalem, 1971.)

Sytinskiy, A. D., and V. P. Tripol'nikov, Some results of investigations of the natural vibrations of ice fields of the central Arctic, *Izv. Akad. Nauk. SSSR, Ser. Geofiz., 4*, 615–621, 1964.

Wadhams, P., Measurement of wave attenuation in pack ice by inverted echo sounding, Proceedings of the International Sea Ice Conference, pp. 255–260, Nat. Res. Counc. of Iceland, Reykjavik, 1972.

Wadhams, P., Attenuation of swell by sea ice, *J. Geophys. Res., 78*(18), 3552–3563, 1973*a*.

Wadhams, P., The effect of a sea ice cover on ocean surface waves, Ph.D. dissertation, 223 pp., Univ. of Cambridge, Cambridge, 1973*b*.

(Received March 5, 1975;
revised May 30, 1975;
accepted May 30, 1975.)